Supplementary Information

Role of Ethanol in Sodalite Crystallization in an Ethanol-Na_2O-Al_2O_3-SiO_2-H_2O System

Yi Huang,[a,b] Jianfeng Yao,[a] Xueyi Zhang,[b] Chunhua (Charlie) Kong,[c] Huiyong Chen,[b] Dongxia Liu,[b] Michael Tsapatsis,[b] Matthew R. Hill,[d,e] Anita J. Hill,[e] and Huanting Wang*[a]*

[a] Department of Chemical Engineering, Monash University, Clayton, VIC, 3800, Australia, [b] Department of Chemical Engineering and Materials Science, University of Minnesota, 421 Washington Avenue SE, Minneapolis, MN 55455, USA, [c] Electron Microscope Unit, University of New South Wales, Sydney, NSW, 2052, Australia, [d] School of Chemistry, University of Melbourne, Victoria 3010, Australia, and [e] Commonwealth Scientific and Industrial Research Organization (CSIRO), Materials Science and Engineering, Private Bag 33, Clayton South, VIC 3169, Australia.

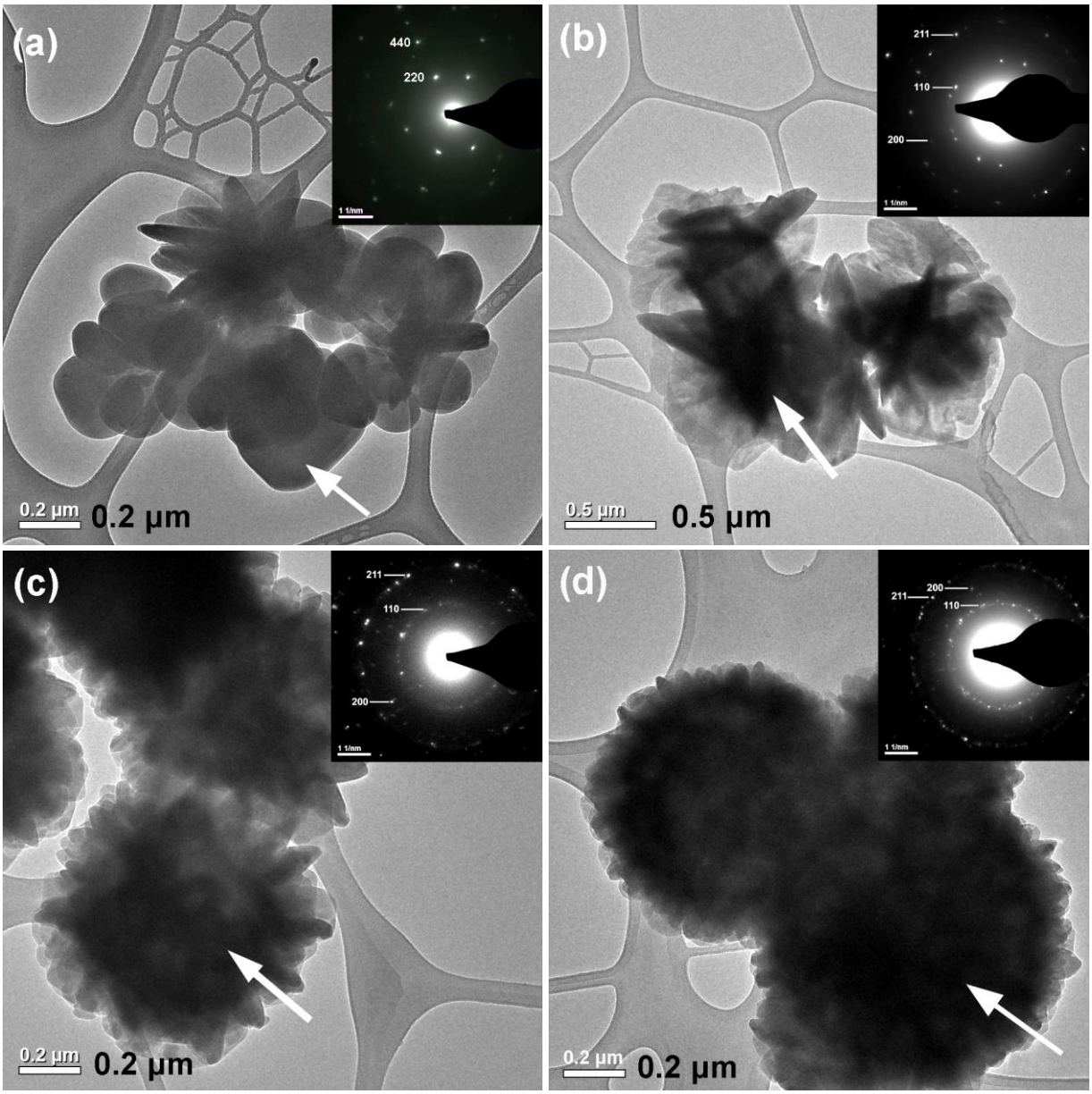

Fig. S1. TEM images and SAED patterns of (a) SOD-0Et(3), (b) SOD-0Et(5), (c) SOD-4Et(3), and (d) SOD-8Et(3). The arrows in each TEM image point to the zeolite A/sodalite particles from where the SAED patterns were collected.

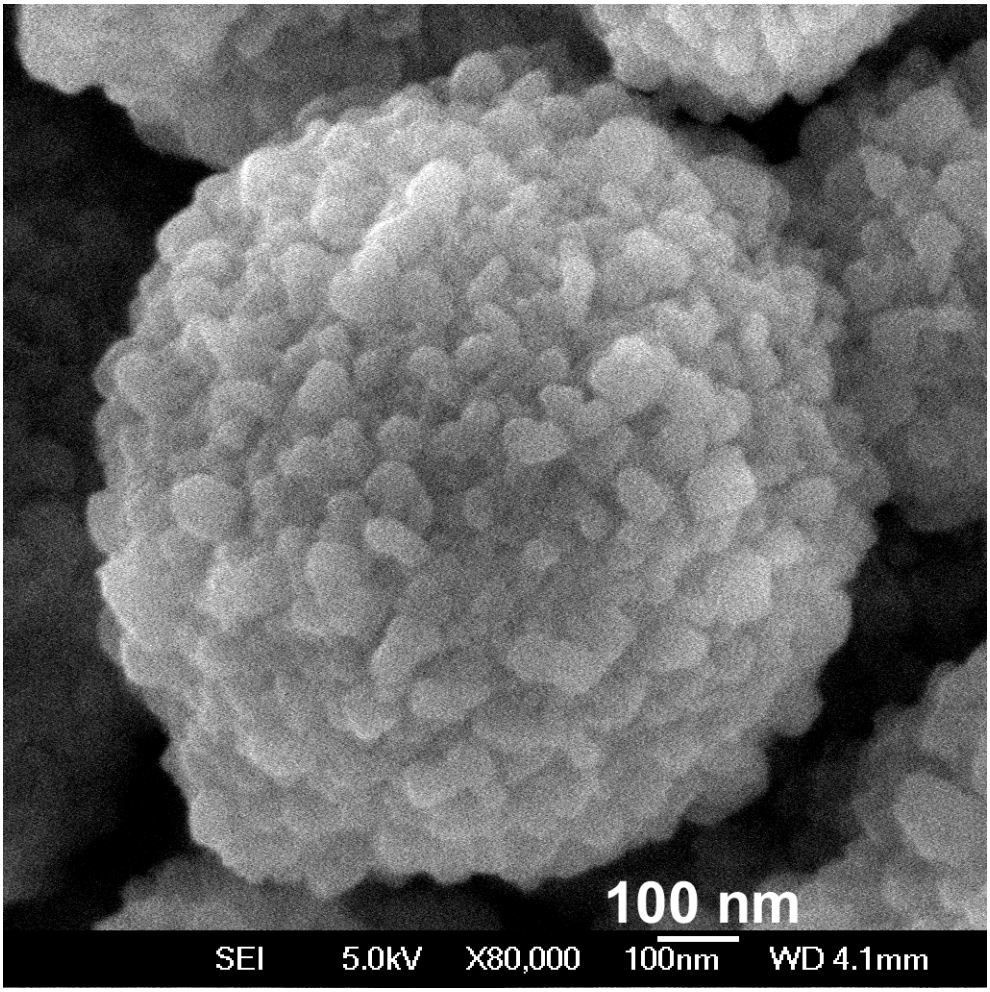

Fig. S2. SEM images of SOD-16Et(2) at high magnification.

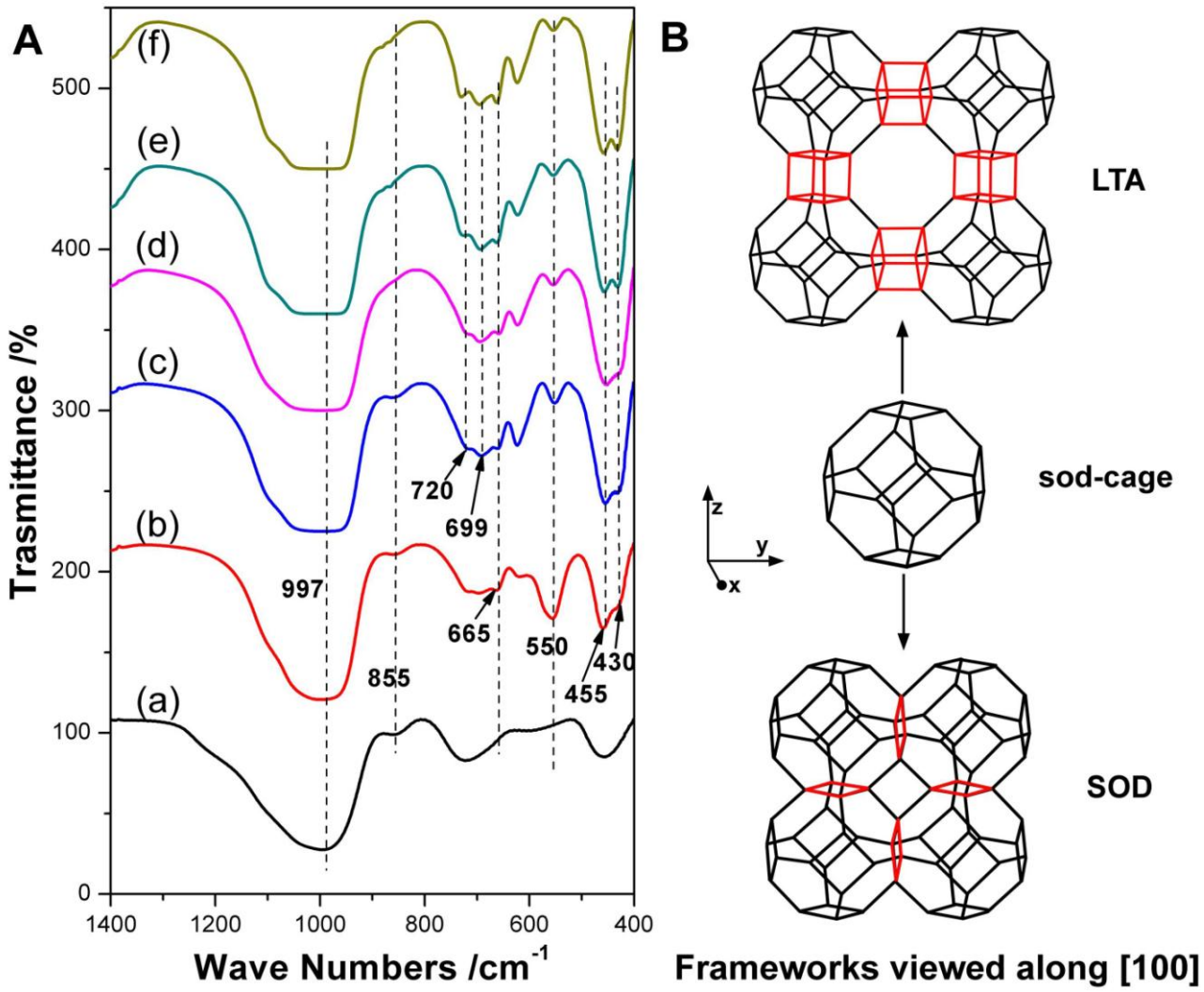

Fig. S3. (A) IR spectra of specimens SOD-16Et(*t*). (a) SOD-16Et(0.5), (b) SOD-16Et(2), (c) SOD-16Et(3), (d) SOD-16Et(5), (e) SOD-16Et(16), and (f) SOD-16Et(35). (B) Representations of the frameworks of zeolite A (LTA type) and sodalite (SOD type), displaying how they are constructed from the sodalite (sod) cage. The red colored units in LTA and SOD frameworks present the double-4-ring and the simple-4-ring connections, respectively.

The spectrum of sample SOD-16Et(0.5) after 0.5 h reaction shows broad absorption bands in the range of 400 -520 cm^{-1} and 630 - 800 cm^{-1}, which are ascribed to typical of amorphous sodium aluminosilicate species (Fig. S3A, (a)).[1] This characteristic amorphous sodium aluminosilicates IR spectrum remained after 1 h reaction time (data not shown here), in good agreement with XRD result. Fig. S3A, (b) shows the IR spectrum of SOD-16Et(2) with the appearance of an intensified absorption band at 550 cm^{-1} which could

be assigned to the external vibration mode of double-4-ring units (D4R), the characteristic band for zeolite A framework.[2-3] In addition, the absorption bands peaked at about 997 cm^{-1} are due to internal vibration of T-O-T (T = Si, Al) asymmetric stretching, and the bands at 720, 699, and 665 cm^{-1} can be assigned to the symmetric stretch of T-O-T. The internal vibrations of T-O-T bending modes also appear at about 455 and 430 cm^{-1}. It is noted that the absorption bands at 997, 720, 699, 665, 455 and 430 cm^{-1} are also characteristic of sodalite framework,[4-5] as shown in Fig. S3A, (c – f). The representations of zeolite A and sodalite frameworks are displayed in Fig. S3B. In zeolite A, each SOD-cage is connected to six nearest neighboring sod-cages through double 4-rings (D4R); whereas these D4R connections are substituted by the simple 4-rings in sodalite. Therefore, by distinguishing the typical variation mode of D4R, it would be able to trace the zeolite A qualitatively in the system where the phase transformation (zeolite A to sodalite) occurs. In our system, a trace amount of zeolite A phase is present throughout 3 and 65 h reaction times, as indicated by the presence of gradually weakened absorption band of D4R. However, this is hard to be detected by routine XRD scan (1 °/min at a step size of 0.02) due to its extremely low content in the samples. The IR spectra also show the gradually intensified characteristic sodalite absorption bands, as would be expected from longer crystallization times. The broad band centered at 850 cm^{-1} can be assigned to the silanol (Si-OH) bending mode, which is commonly observed in hydrosodalite.[3-4]

References

1. V. P. Valtchev, K. N. Bozhilov, *J. Phys. Chem. B,* 2004, **108**, 15587-15598.
2. R. M. Barrer, *Hydrothermal Chemistry of Zeolites*, Academic Press, London, 1982.
3. D. W. Breck, *Zeolite Molecular Sieves: structure, chemistry and use*, John Wiley & Sons, New York, 1974.
4. W. Fan, K. Morozumi, R. Kimura, T. Yokoi, T. Okubo, *Langmuir* 2008, **24**, 6952-6958.
5. J. F. Yao, H. T. Wang, K. R. Ratinac, S. P. Ringer, *Chem. Mater.,* 2006, **18**, 1394-1396.

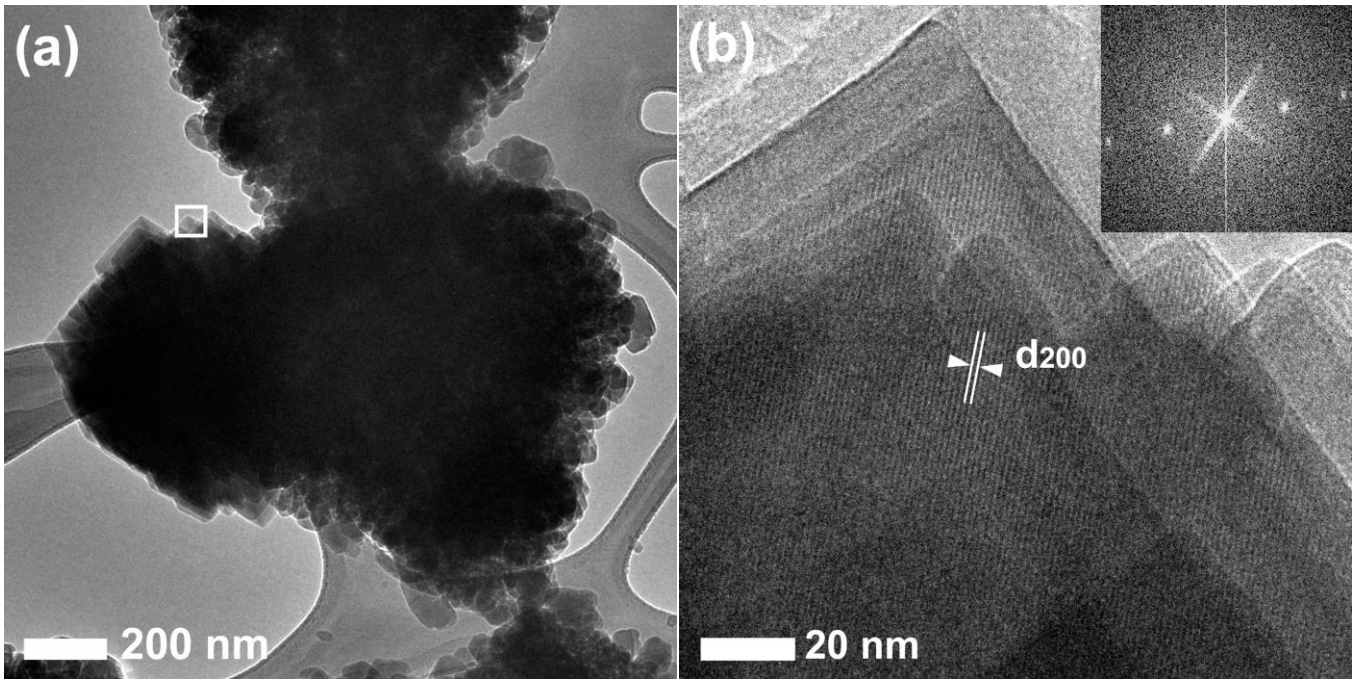

Fig. S4. (a) TEM image shows the agglomerate of cubic zeolite A crystals and spherical sodalites in sample SOD-16Et(2). The region highlighted by a square in panel (a) is shown in the HRTEM (b). The corresponding FFT (top inset in (b)) showing spots (d = 6.2 Å, (200) planes from LTA structure) and lattice fringes displayed in (b) both confirm the LTA-type framework structure of the cubic crystals.

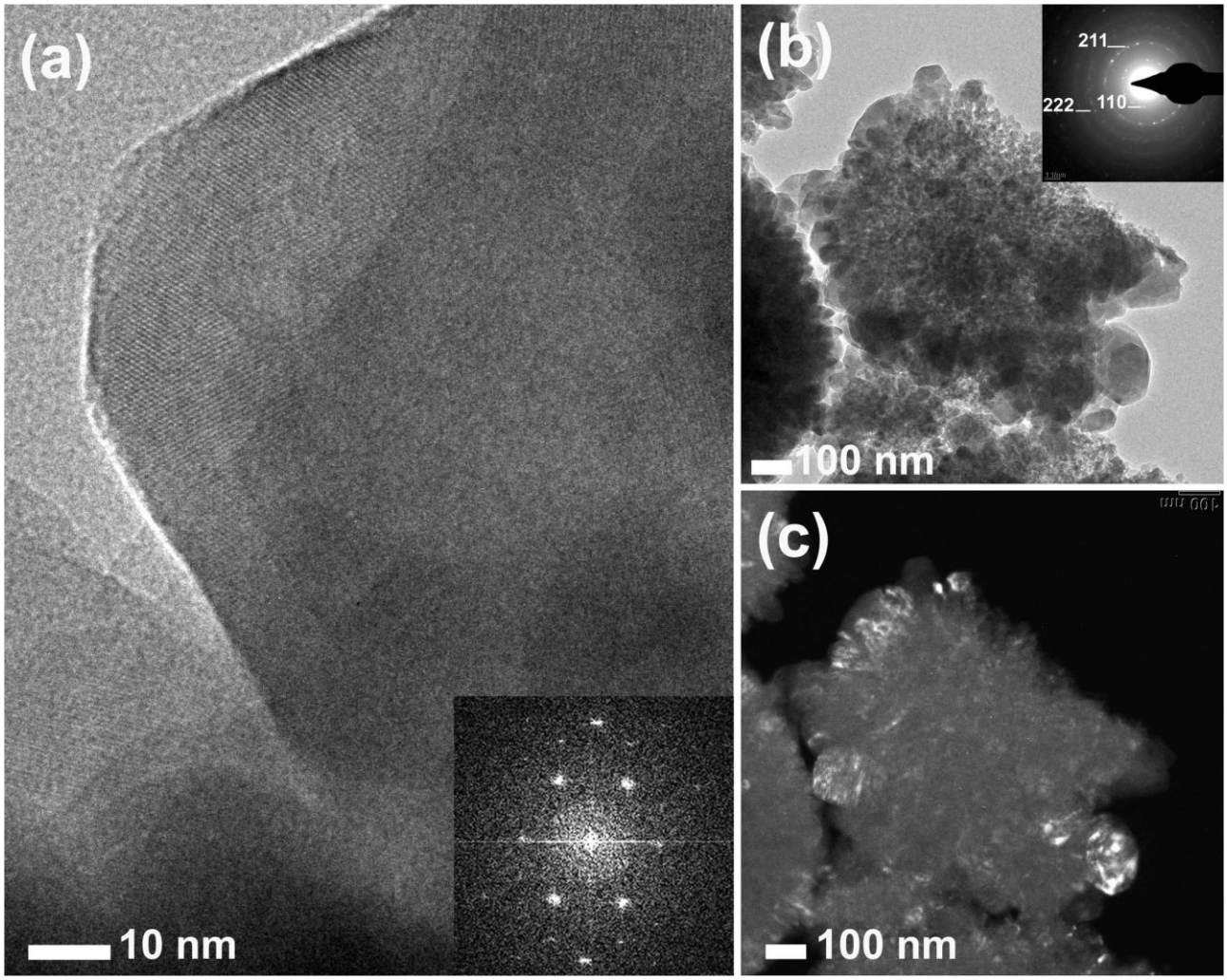

Fig. S5. TEM images of SOD-16Et(3). Panels (a) is the high resolution (HR) TEM image captured in shell regions of the spherical particles. Panels (b) and (c) are TEM and dark-field TEM images, respectively. The Fast Fourier Transform (FFT) of the whole HRTEM image is displayed in bottom-right corner of panel (a). The inset in panel (b) is the selected area electron diffraction (SAED) pattern collected from the broken particle.

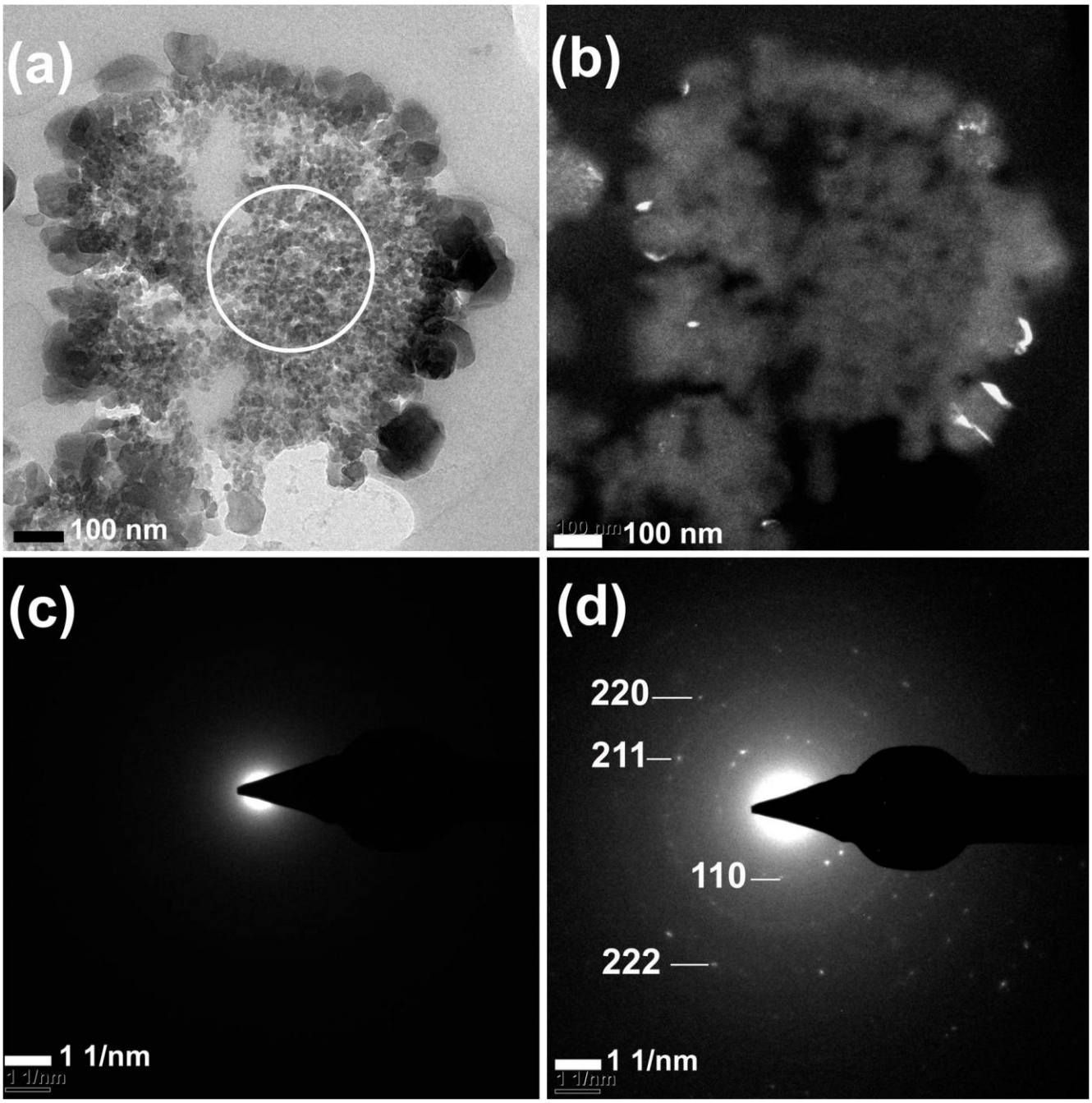

Fig. S6. TEM (a) and DF-TEM (b) images of the sectioned sodalite particle (SOD-16Et(16)). (c) and (d) are SAED patterns taken from the interior (marked by the cycle in (a)) and the entire particle, respectively.

TEM (a) images reveal the crystallization of nanocrystalline sodalites takes place in the shell region, as also confirmed by DF-TEM image (b). SAED examinations (c - d) reveal that the particle interior is amorphous (c) whereas the entire section gives a polycrystalline SAED pattern (d), which provides strong evidence for surface crystallization.

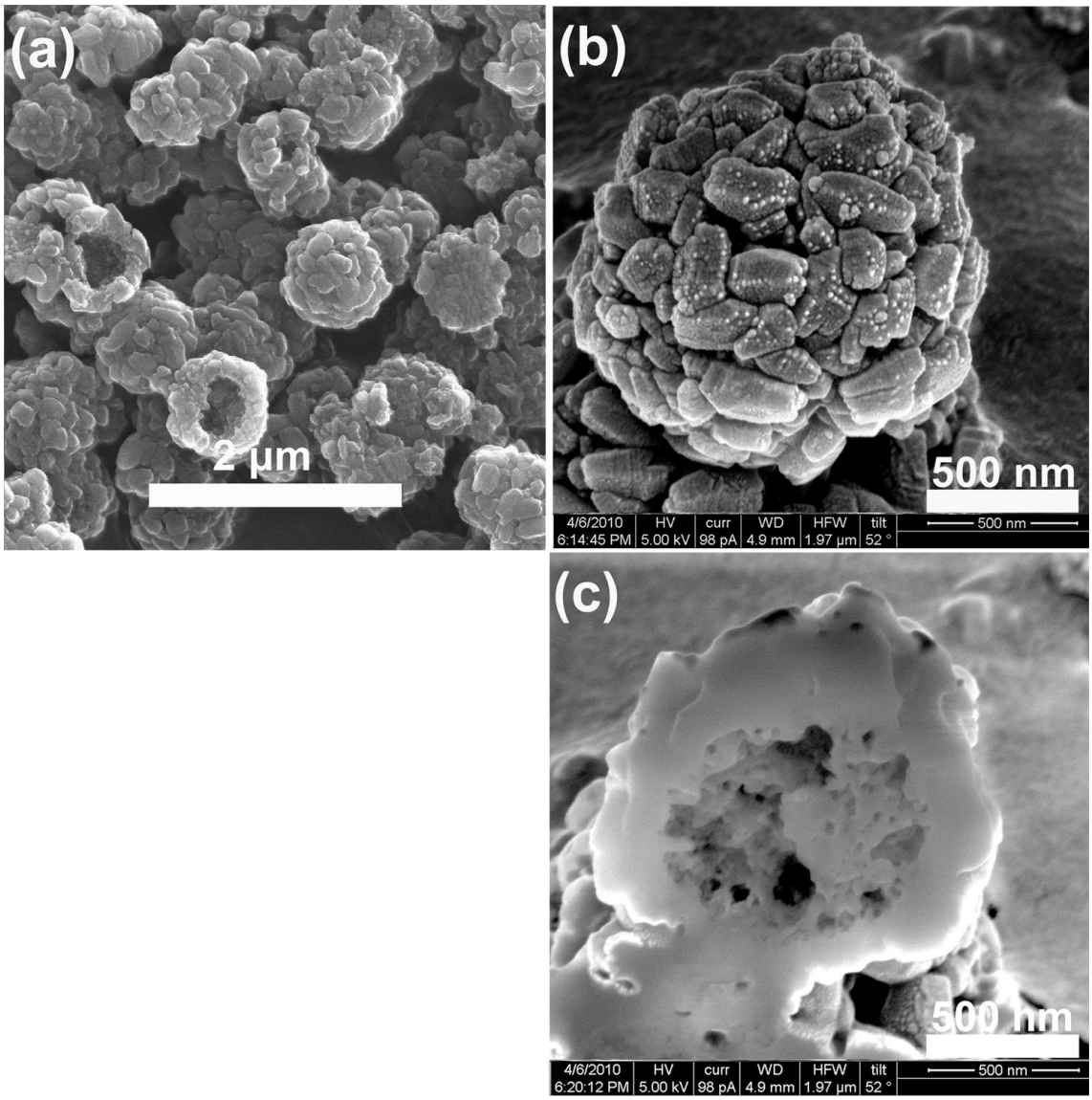

Fig. S7. SEM (a - b) and FIB-SEM images (c) of SOD-16Et(65).

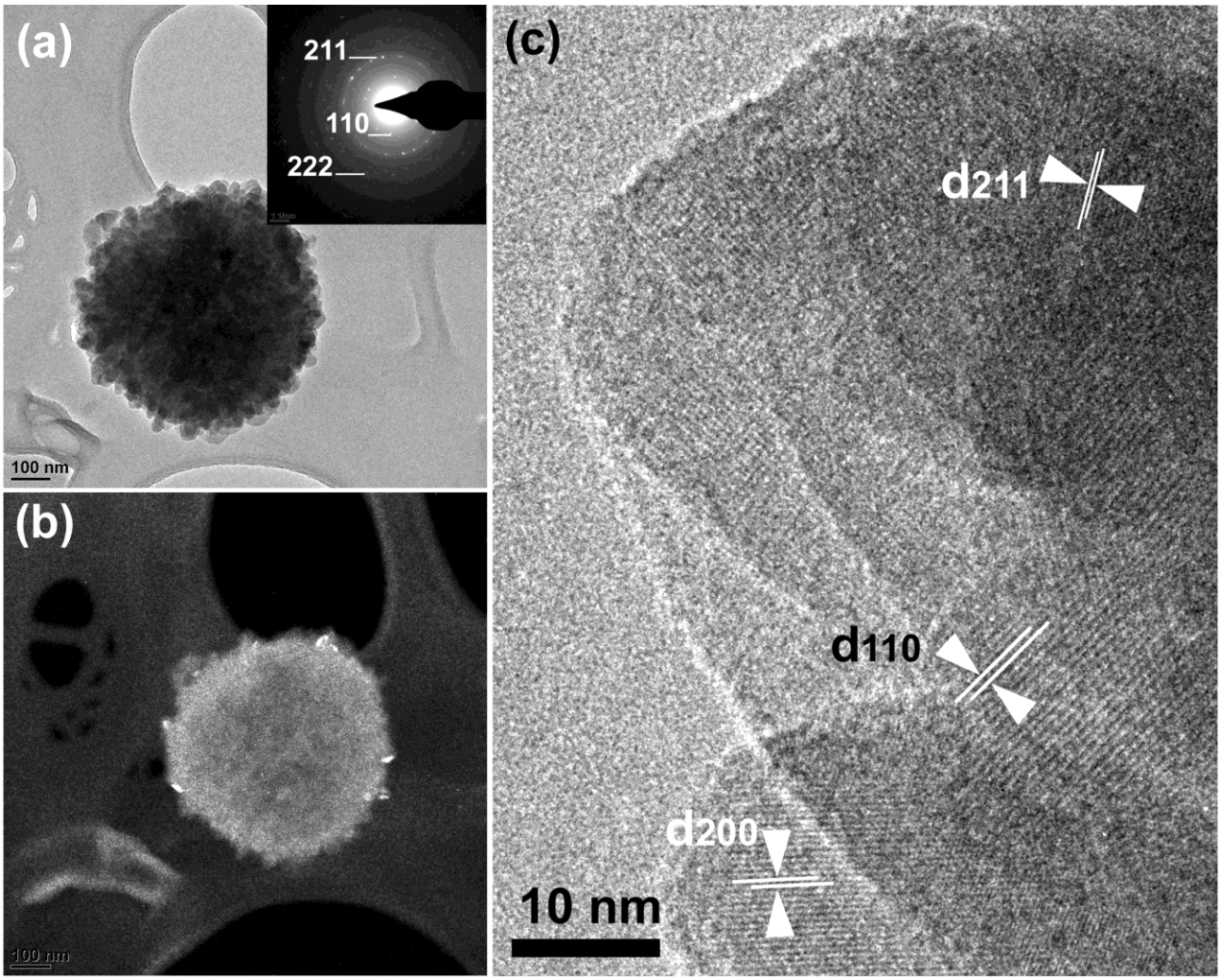

Fig. S8. TEM images (a - c) of SOD-32Et(3).

TEM image (a) shows a spherical sodalite particle with nanocrystalline shell crystals in the size range of 20 – 80 nm. The inset SAED pattern collected from the entire particle reveals that it is polycrystalline in nature. Dark-field TEM (b) obtained from a single particle shows many fine bright spots near the surface, confirming the presence of many small crystals in the shell region. HRTEM image (c) captured in shell regions of the spherical particles displayed distinct lattice fringes (highlighted by the paralleled lines) with d_{110} (6.25 Å), d_{200} (4.42 Å), and d_{211} (3.61 Å) spacings, indicating the smaller shell-crystals are highly crystallized. Note that the appearance of lattice fringes with different directions is because of the overlap of several nanocrystalline sodalite domains with different orientations.

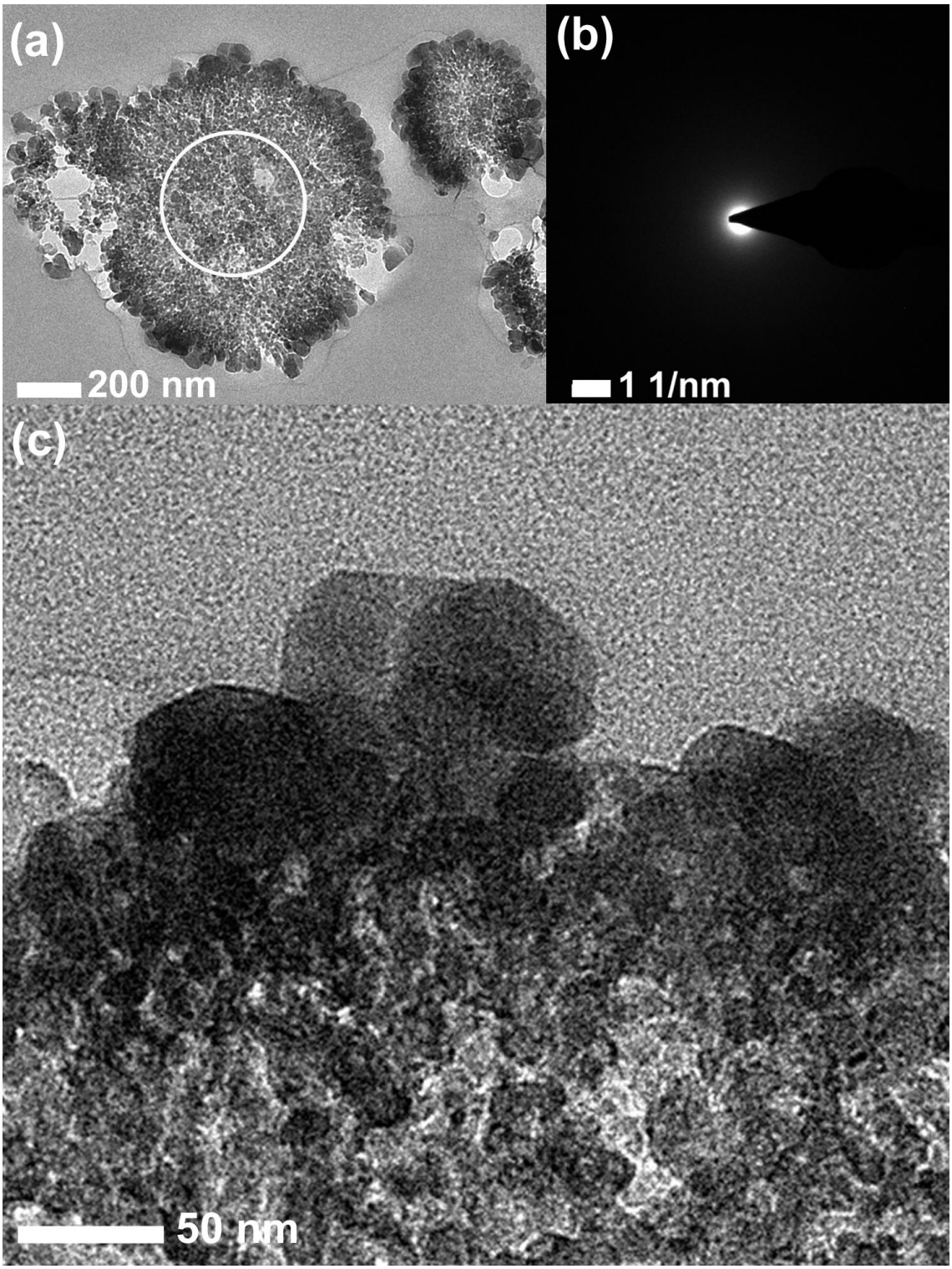

Fig. 9 (a) TEM images of the sectioned sodalite particle (SOD-32Et(3)). (b) SAED pattern confirms that the particle interior (highlighted by the cycle in panel (a)) is amorphous. (c) HR-TEM image shows the features near the core-shell boundaries.

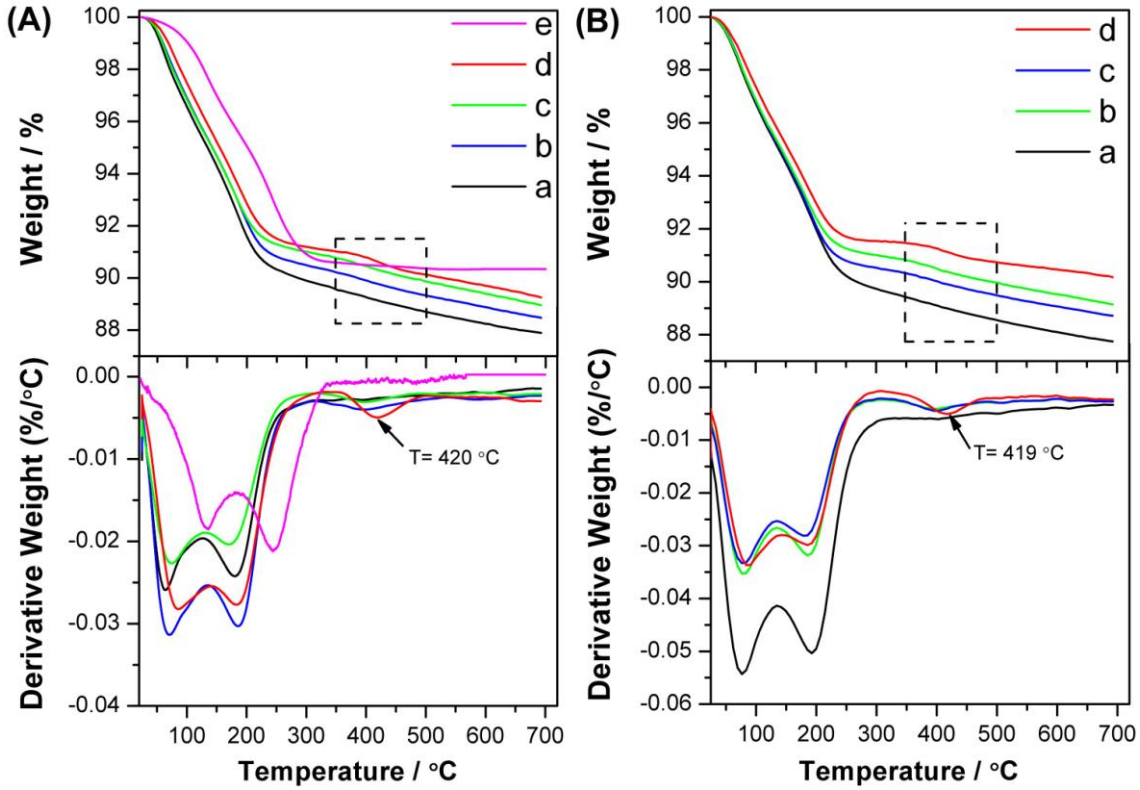

Fig. S10. TGA-DTG curves of sodalite specimens obtained in flowing air (A) and nitrogen (B). (a) SOD-16Et(3), (b) SOD-16Et(16), (c) SOD-16Et(45), (d) SOD-16Et(65), and (e) SOD-0Et(16) (SOD phase). The dashed rectangles present in graphs A and B show a temperature range of 350 - 500 °C, where the decomposition of ethanol probably occurs. The arrows in the DTG plots point to the peak temperatures obtained during this process.

Table S1. Mass loss of sodalite samples obtained by TG analysis under air and nitrogen conditions

	Air	Nitrogen
Sample	Total mass loss (%)	Total mass loss (%)
SOD-0Et(16)	9.55	-
SOD-16Et(3)	12.25	12.11
SOD-16Et(16)	11.53	11.18
SOD-16Et(45)	11.04	10.50
SOD-16Et(65)	10.75	9.83

As shown in Fig. S10, the samples prepared with longer reaction time possess a lower mass loss, confirming the reduced amount of amorphous phase in the samples. A slight decreased mass loss (0.15 - 0.92 %) was obtained when the flowing gas was switched from air to nitrogen (Table S1), probably due to

the incomplete combustion of occluded ethanol in N_2 atmosphere. Moreover, the TG-DTG curves revealed that all samples had the mass loss mainly before 250 °C, which was related to desorption of structural water and loosely bonded ethanol. A further decrease in mass could be attributed to the condensation of hydroxyl groups associated with nanocrystalline hydrosodalite. The mass loss by ethanol-free pure hydrosodalite SOD-0Et(16) is 9.55 % (Fig. S10A), owing to the removal of structural water.[1] According to the corresponding DTG curve, a higher temperature of around 330 °C is required to accomplish this process. This is because the interaction between water and sodalite structure is much stronger in the absence of co-solvent ethanol. Closer examination of the DTG curves revealed that a secondary mass loss appears with a peak temperature of about 420 °C and became more apparent in the samples prepared with longer crystal growth time; this is probably related to the decomposition of ethanol molecules. It has been reported that ethanol is a weak SDA (as compared with tetraalkylammonium cations) in the synthesis of MFI-type zeolites (e.g. ZSM-5).[2-4] The reactive hydroxyl groups of ethanol molecules could strongly bond to the zeolite structure during the templating process and thus remain in the micro-channels of the zeolite structures. Moreover, the temperatures ranging from 200 °C to 450 °C were shown to be related to the combustion of structural ethanol.[3] Accordingly a strongly exothermic peak should appear in the differential thermal analysis (DTA) curves. However, a small mass loss (~ 1 wt%) was found at higher temperatures, and in a broader temperature range (350 - 500 °C) in our case (Fig. S10A, B), implying the interaction between ethanol and sodalite structure is much stronger.

References

1 J. F. Yao, H. T. Wang, K. R. Ratinac, S. P. Ringer, *Chem. Mater.*, 2006, **18**, 1394-1396.

2 E. Costa, M. A. Uguina, A. Delucas, J. Blanes, *J. Catal.*, 1987, **107**, 317-324.

3 X. L. Seoane, A. Arcoya, J. A. Gonzalez, N. Travieso, *J. Mater. Sci.*, 1991, **26**, 172-176.

4 M. A. Uguina, A. Delucas, F. Ruiz, D. P. Serrano, *Ind. Eng. Chem. Res.*, 1995, **34**, 451-456.

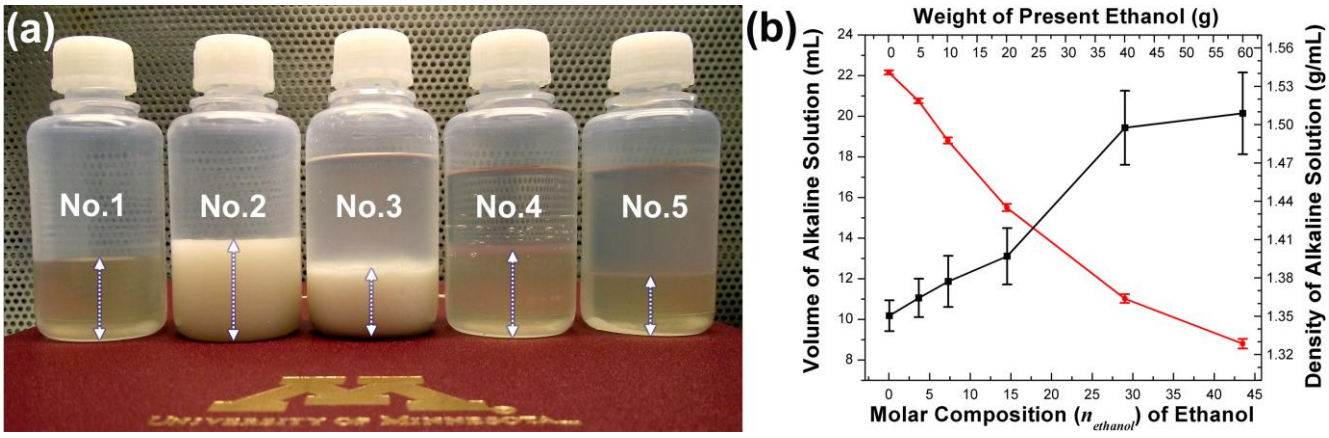

Fig. S11. (a) Photographs of alkaline solution ($3.61Na_2O$: $1.00Al_2O_3$: $52.84H_2O$, molar ratio) (No.1), freshly prepared zeolite gel ($3.61Na_2O$: $1.00Al_2O_3$: $52.84H_2O$: $1.20SiO_2$, molar ratio) (No.2), zeolite gel - ethanol mixture ($3.61Na_2O$: $1.00Al_2O_3$: $52.84H_2O$: $1.20SiO_2$: $16C_2H_6O$, molar ratio) after 24 h mixing (No.3), alkaline solution-ethanol mixture before stirring (No.4), and final alkaline solution-ethanol mixture after 24 h stirring (No.5). The weights of alkaline solution, colloidal silica, and ethanol used here were 29.91, 6.5 and 20 g, respectively. The dotted lines with double arrows denote the volume change of the bottom solution after each step. (b) Plot of the final volume and density of the alkaline solutions (after one day mixing) as a function of ethanol added ($n_{ethanol}$ = 0, 4, 8, 16, 32, and 48, corresponding to the addition of 0, 5, 10, 20, 40, and 60 g of ethanol, respectively). The densities of bottom alkaline solutions after extraction process were estimated by the equation: ρ = m/V. Before measuring, the supernatant was carefully removed. For each composition between 10 and 12 analyses were performed.

Fig. S11a shows a photograph of the synthesis solutions/mixtures prepared under different conditions. Upon visual observation, the complete zeolite synthesis mixture (No.3 bottle) appears to be a two-phase mixture with a significantly reduced amount of zeolite gel phase at the bottom. It is worth mentioning that the zeolite gel (No.2) was immiscible with ethanol even after extended agitation. Without stirring, the gel phase quickly precipitated into the bottom. After thoroughly mixing, a distinct volume reduction of the bottom gel phase was observed. This phenomenon is probably due to the significant change in the gel composition as the zeolite precursor is more soluble in water than ethanol (e.g., NaOH solubility in water is 111 g/mL at 20 °C while NaOH solubility in ethanol is 13.9 g /mL.). To further examine the influence of

the ethanol content on the density of the bottom synthesis solution, 29.91 g of the alkaline solution instead of the zeolite gel was thoroughly mixed with an increasing amount of ethanol at room temperature for 24 h. Fig. S11b shows the volume and density of the final alkaline solution as a function of the weight/volume of ethanol added. Apparently, the increase in $n_{ethanol}$ from 4 to 48 leads to almost a linear reduction of the volume of alkaline solution, confirming the gradual concentration of the bottom alkaline solution. Moreover, the density of the alkaline solution after complete mixing increased simultaneously (Fig. S11b). Therefore, the higher degree of supersaturation of sodium aluminates would be expected from the more concentrated alkaline solution. A typical demonstration of the ethanol extraction phenomenon is shown in Fig. S11a. The liquid in the first bottle (No.1) is the freshly prepared alkaline solution with an amount of 29.91 g. Right after the addition of ethanol (20 g), the interface between alkaline solution and ethanol became cloudy, indicating the concentration process began immediately (Fig. S11a, No.4). After vigorous agitation for 24 h, the final volume of alkaline solution reduced to be about 70% of its initial volume (Fig. S11a, No.5). The concentrated alkaline solution with reduced volume still remained at the bottom of the bottle. Substitution of the zeolite gel for alkaline solution might further enhance the concentration process due to the condensation of silicon and sodium/aluminum species in the synthesis zeolite gel. Therefore, it is reasonable to conclude that more concentrated zeolite gel was obtained after mixing with more ethanol.